

# Noise Removal Technique in Near-Field Millimeter-Wave Cylindrical Scanning Imaging System

Xin Wen<sup>1, 2, 3, \*</sup>, Feng Nian<sup>2, 3</sup>, Yujie Yang<sup>3</sup>, and Keming Feng<sup>2, 3</sup>

**Abstract**—The accuracy of scattering measurements in near-field millimeter-wave cylindrical scanning imaging system is often degraded by the contamination from additive noise and clutter. Thus, efficient noise and clutter removal technique is necessary to achieve accuracy improvement. This paper proposes an independent component analysis denoising algorithm, which relies on the assumption of statistical independence of the sources, where high order statistical properties are used. In the algorithm, the virtual noise components are incorporated into the independent component analysis model, which expands original one-dimensional observation to virtual multi-dimensional observations. The computationally efficient sources estimation technique is presented, based on the joint diagonalization of fourth order cumulant matrix. The high speed millimeter-wave near-field cylinder scanning imaging system is set up to verify the denoising results in the range profiles, three-dimensional scatter intensity and two-dimensional projection images. Compared with three different noise models, the results indicate that the denoising algorithm shows both feasibility and validity in the near-field millimeter-wave cylindrical scanning imaging system.

## 1. INTRODUCTION

The millimeter-wave can penetrate common clothing materials and is reflected by human body and by concealed items. Also, the radiant power required in near-field imaging is in milliwatt level, which is 1/1000 of the transmission power of an ordinary mobile phone, relieving the worry about adverse effect on the human body. These characteristics make the near-field millimeter-wave cylindrical scanning imaging techniques a good candidate to be developed for personnel surveillance application, including the detection of concealed weapons, explosive, drugs and other contraband materials. The imaging system is based on the cylindrical synthetic aperture radar (CSAR) technology [1], which scans the surface of human body through high speed rotating. The radar transceiver transmits the broadband signal to provide high resolution, which limits the bandwidth of intermediate frequency filter. The improvements in measurements hardware, residual noise can still make low-level returns, which deteriorates the measurements [2]. Therefore, efficient and robust denoising algorithm is required.

The noise sources of the imaging system include: system burst interference, system measuring noise, reflection from system mechanical supporting part, mutual coupling of antenna array, mutual interference between measuring objects and mechanical supporting part, etc. [3]. The traditional denoising methods often rely on the relative detailed knowledge of the original signal types or the accurate identification of the signal transmission system, which make the traditional methods difficult to be applied in complex electromagnetic environment, especially in near-field measurements condition.

According to [3], the noise of the imaging system can be reduced through coherent averaging. However, this method requires three preconditions: 1) the mean of the noise is zero; 2) the noise is

---

*Received 29 May 2014, Accepted 17 August 2014, Scheduled 23 August 2014*

\* Corresponding author: Xin Wen (wenxin\_203@163.com).

<sup>1</sup> Information Engineering School, Communication University of China, Beijing 10024, P. R. China. <sup>2</sup> Science and Technology on Metrology and Calibration Laboratory, Beijing 100854, P. R. China. <sup>3</sup> Beijing Institute of Radion Metrology & Measurement, Beijing 100854, P. R. China.

Gaussian random stationary process; 3) each observation is not relative, which limit the usage of the method. Another denoising method is based on the range-gating and background subtraction [4, 5]. This method has been successfully applied in reducing the noise due to direct backscatter from coherent sources. This method can not be applied in the actual imaging system, owing to the fact that the low repeatability of the imaging system, and the method is not effective to handle with the noise from electromagnetic interaction. The more effective denoising method is using Fourier or spectral estimation to separate target returns from the noise [6]. The separation is implemented by spectrum or spectral domain transform with the corresponding filters or subtraction. However, this method can not separate targets from the noise satisfyingly especially within the filters, and the signal processing will also introduce noise. An alternate idea is to separate the desired targets from the noise based on the assumption that the targets and noise have different statistical properties of the observed data. Accordingly, we consider using the independent component analysis (ICA) algorithm to address this problem [7]. In recent years, ICA algorithm has become a hot issue in signal processing field, especially, used as a kind of effective denoising technique. It has been widely used in many fields, including image processing, biomedicine, radar, sonar, communication, speech signal processing and earthquake prediction, etc.

## 2. ICA DENOISING ALGORITHM

### 2.1. The Principle of ICA

ICA is a statistical model where the observed data is expressed as a linear transform of latent variables. We may express the model as

$$\mathbf{x} = \mathbf{A}\mathbf{s} + \mathbf{n} = \mathbf{y} + \mathbf{n} \quad (1)$$

where  $\mathbf{x} = (\mathbf{x}_1, \dots, \mathbf{x}_m)$  is the vector of observed random variables.  $\mathbf{s} = (\mathbf{s}_1, \dots, \mathbf{s}_n)$  is the sources vector of statistically independent components and not Gaussian signals.  $\mathbf{A}$  is an unknown  $m \times n$  constant mixing matrix. The vector  $\mathbf{n}$  is defined as additive noise, which is normally distributed and independent from the sources. For any whitening matrix  $\mathbf{W}$ , the whiten condition is  $\mathbf{I}_n = \mathbf{W}\mathbf{R}_y\mathbf{W}^H$ , then it exists a unitary matrix  $\mathbf{U}$  such that  $\mathbf{W}\mathbf{A} = \mathbf{U}$ . As a consequence, matrix  $\mathbf{A}$  can be factored as

$$\mathbf{A} = \mathbf{W}^\# \mathbf{U} = \mathbf{W}^\# [\mathbf{u}_1, \dots, \mathbf{u}_n] \quad (2)$$

The process reduces the dimension of  $m \times n$  mixing matrix  $\mathbf{A}$  to a unitary  $n \times n$  matrix  $\mathbf{U}$ . The whitened process  $\mathbf{z} = \mathbf{W}\mathbf{x}$  still obeys a linear model

$$\mathbf{z} \stackrel{\text{def}}{=} \mathbf{W}\mathbf{x} = \mathbf{W}(\mathbf{A}\mathbf{s} + \mathbf{n}) = \mathbf{U}\mathbf{s} + \mathbf{W}\mathbf{n} \quad (3)$$

To any given  $n \times n$  matrix  $\mathbf{M}$ ,  $\mathbf{Q}_z(\mathbf{M})$  is the fourth order cumulant matrix of  $\mathbf{z} \cdot [\mathbf{Q}_z(\mathbf{M})]_{ij}$  is defined as

$$[\mathbf{Q}_z(\mathbf{M})]_{ij} = \sum_{k=1}^n \sum_{l=1}^n \text{cum}[\mathbf{z}_i, \mathbf{z}_j^*, \mathbf{z}_k, \mathbf{z}_l^*] \cdot m_{kl} \quad 1 \leq i, \quad j \leq n \quad (4)$$

where  $\text{cum}[\mathbf{z}_i, \mathbf{z}_j^*, \mathbf{z}_k, \mathbf{z}_l^*]$  is the cumulant of the entries in  $i$ th and  $k$ th rows with  $j$ th and  $l$ th columns of  $\mathbf{z}$  [8].  $m_{kl}$  is the  $(k, l)$ th entry of matrix  $\mathbf{M}$ . When taking  $\mathbf{M} = \mathbf{b}_l \mathbf{b}_k^*$ ,  $\mathbf{b}_k^*$  denotes the  $n \times 1$  vector with 1 in  $k$ -th position and 0 elsewhere.  $\mathbf{Q}_z(\mathbf{M})$  can be seen as a linear combination of “parallel cumulant slices” with the entries of  $\mathbf{M}$  as coefficient. The “parallel set”  $\mathbf{N}^p$  can be defined as the set of all the parallel slices

$$\mathbf{N}^p = \{ \mathbf{Q}_z(\mathbf{b}_l \mathbf{b}_k^*) \mid 1 \leq k, l \leq n \} \quad (5)$$

Using the cumulant properties of Gaussian rejection, additivity and multi-linearity,  $\mathbf{Q}_z(\mathbf{M})$  can be rewritten as

$$\mathbf{Q}_z(\mathbf{M}) = \sum_{p=1}^n k_p \mathbf{u}_p^* \mathbf{M} \mathbf{u}_p \mathbf{u}_p^* = \mathbf{U} \mathbf{\Lambda}_M \mathbf{U}^H \quad (6)$$

where  $\mathbf{\Lambda}_M = \text{diag}(k_1 \mathbf{u}_1^* \mathbf{M} \mathbf{u}_1, \dots, k_n \mathbf{u}_n^* \mathbf{M} \mathbf{u}_n)$ ,  $k_p$  is the kurtosis of the  $p$ th source, then  $k_p = \text{cum}(\mathbf{s}_p, \mathbf{s}_p^*, \mathbf{s}_p, \mathbf{s}_p^*)$ . The Equation (6) shows that any cumulant matrix can be diagonalized by  $\mathbf{U}$ . There are many methods applied in the determination of  $\mathbf{U}$ . A joint diagonalization is a precisely and

effective method [9]. The joint diagonalization of the set  $\mathbf{N}^p$  is defined as follows, the determination of  $\mathbf{U}$  as a unitary maximizer of the criterion

$$C(\mathbf{V}, \mathbf{N}^p) = \sum_{r=1}^n |\text{diag}(\mathbf{V}^H \mathbf{N}^p \mathbf{V})|^2 \quad (7)$$

where  $|\text{diag}(\cdot)|$  is the norm of the vector built from the diagonal of the matrix argument. The joint diagonalizer of  $\mathbf{N}^p$  is essentially equal to  $\mathbf{U}$  [9]. The Jacobi technique can be extended to the joint diagonalization of the matrix [10]. In order to reduce the computation, the set  $\{\mathbf{u}_p \mathbf{u}_q^* | 1 \leq p, q \leq n\}$  satisfies the properties of orthonormality, then  $\mathbf{Q}_z(\mathbf{u}_p \mathbf{u}_p^*) = k_p \mathbf{u}_p \mathbf{u}_p^*$ , while  $\mathbf{Q}_z(\mathbf{u}_p \mathbf{u}_q^*) = 0$  for  $p \neq q$ . By taking into account the  $n$  most significant eigenpairs are needed,  $\mathbf{Q}_z(\mathbf{u}_p \mathbf{u}_q^*)$  is made of  $n(n-1)$  zeros eigenvalues and  $n$  eigenvalues equal to the kurtosis of the sources. After ordering the eigenvalues of magnitude, the eigen-set of  $\mathbf{Q}_z(\mathbf{u}_p \mathbf{u}_q^*)$  is

$$\mathbf{N}^e = \{\lambda_r \mathbf{M}_r | 1 \leq r \leq n\} \quad (8)$$

This reduced set  $\mathbf{N}^e$  together with the extended Jacobi technique makes the maximization of  $C(\mathbf{V}, \mathbf{N}^e)$  computationally attractive.

### 2.2. Virtual Noise ICA Model

According to the fact that higher than the second order cumulant of Gaussian noise is zero, the virtual noise ICA model can effectively restrain Gaussian noise on the basis of Equation (1). When the mixing matrix  $\mathbf{A}$  degenerated to constant 1, the Equation (1) becomes one-dimensional noisy observation expression [11, 12]. When dealing with one-dimensional observation, it must introduce appropriate virtual variables to expand to multi-dimensional observations [13]. When adding external  $M$  kinds of noise, such as  $\mathbf{n} = \sum_{i=1}^M a_i \mathbf{n}_i$ ,  $a_i$  is the weight of the  $i$  kind noise in the observations. The noisy observations

model is transformed to  $\mathbf{x} = \mathbf{s} + \mathbf{n} = \mathbf{s} + \sum_{i=1}^M a_i \mathbf{n}_i$ . If introducing reference noise  $\mathbf{n}_1, \mathbf{n}_2, \dots, \mathbf{n}_M$  to form virtual observations vector  $\mathbf{x}_{virtual} = [\mathbf{x}_2, \mathbf{x}_3, \dots, \mathbf{x}_{M+1}]^T$ , the Equation (1) can be rewritten as

$$\mathbf{x} = \mathbf{A}\mathbf{s} \Rightarrow \begin{bmatrix} \mathbf{x}_1 \\ \mathbf{x}_2 \\ \vdots \\ \mathbf{x}_{M+1} \end{bmatrix} = \begin{bmatrix} \mathbf{s} + \sum_{i=1}^M a_i \mathbf{n}_i \\ \mathbf{n}_1 \\ \vdots \\ \mathbf{n}_M \end{bmatrix} = \begin{bmatrix} 1 & a_1 & a_2 & \dots & a_M \\ 0 & 1 & 0 & \dots & 0 \\ 0 & 0 & 1 & \dots & 0 \\ 0 & 0 & 0 & \ddots & 0 \\ 0 & 0 & 0 & \dots & 1 \end{bmatrix} \begin{bmatrix} \mathbf{s} \\ \mathbf{n}_1 \\ \vdots \\ \mathbf{n}_M \end{bmatrix} = \mathbf{B}\mathbf{s} \quad (9)$$

Equation (9) means that introducing the noise components  $\mathbf{n}$  into one-dimensional noisy observation  $\mathbf{x}$ , the sources  $\mathbf{s}$  can be recovered through identifying the virtual full rank mixing matrix  $\mathbf{B}$ . Figure 1 shows the denoising algorithm applied in near-field millimeter-wave cylindrical scanning imaging system.

The original signal collection is the sample data from transceiver, including real signal  $\mathbf{s}$  and noise signal  $\mathbf{n}$ . The process of noise model analysis is to select the proper noise model as the virtual observation  $\mathbf{x}_{virtual}$ . The denoising algorithm is based on higher order cumulants only (hence without second-order

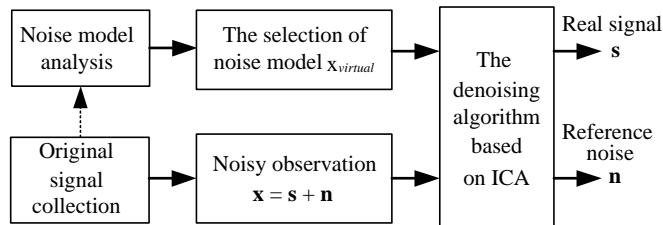


Figure 1. The denoising algorithm schematic diagram.

prewhitening), with the benefit that consistent estimation is possible with modeling the noise as long as it is independent and normally distributed [14]. In order to verify the denoising algorithm, the pulse noise model, white Gaussian noise model, pulse noise plus white Gaussian noise model are used as virtual observation [15].

### 2.3. The Process of ICA Denoising Algorithm

The ICA denoising algorithm based on the principle of ICA and virtual noise ICA model applied in near-field millimeter-wave cylindrical scanning imaging system is divided into 5 steps.

**Step 1.** Load the noisy sample echo data from the imaging system. The noisy original echo data is combined with the measured reference noise to form the virtual observation signal  $\mathbf{x}$ . Form the observation signal covariance  $\mathbf{R}_x$  and compute the whitening matrix  $\mathbf{W}$ .

Step 1 is concerned with two order statistics, which is implemented via eigen decomposition of  $\mathbf{R}_x$ . The estimate  $\hat{\sigma}$  of the noise variance is the average of the  $m - n$  smallest eigenvalues of  $\mathbf{R}_x$ , and denote  $\mu_1, \dots, \mu_n$  the  $n$  largest eigenvalues and  $\mathbf{h}_1, \dots, \mathbf{h}_n$  the corresponding eigenvectors of  $\mathbf{R}_x$ . The whitening matrix is  $\mathbf{W} = [(\mu_1 - \hat{\sigma})^{-1/2}\mathbf{h}_1, \dots, (\mu_n - \hat{\sigma})^{-1/2}\mathbf{h}_n]^H$ .

**Step 2.** Using the parallel slices  $\mathbf{N}^p$  to form the fourth order cumulant matrix  $\mathbf{Q}_z(\mathbf{N}^p)$  of the whitened process  $\mathbf{z}(t) = \mathbf{W}\mathbf{x}(t)$ , compute the  $n$  most significant eignpairs  $\{\lambda_r \mathbf{M}_r | 1 \leq r \leq n\}$ .

Computation of the eigenmatrices amounts to diagonalizing a  $n^2 \times n^2$  matrix made from the elements of  $\mathbf{Q}_z(\mathbf{N}^p)$ . Select the  $n$  most significant eigenpairs to form  $\mathbf{N}^e = \{\lambda_r \mathbf{M}_r | 1 \leq r \leq n\}$ .

**Step 3.** Jointly diagonalize the set  $\mathbf{N}^e = \{\lambda_r \mathbf{M}_r | 1 \leq r \leq n\}$  to estimate unitary matrix  $\mathbf{U}$ . The single-matrix Jacobi techniques is implemented in this step.

**Step 4.** Separate the sources signal from the noise. Estimate  $\mathbf{A}$  as  $\hat{\mathbf{A}} = \mathbf{W}^\# \mathbf{U}$  and estimate the sources components as  $\hat{\mathbf{S}} = \hat{\mathbf{A}}^\# \mathbf{x}$ .

**Step 5.** Import the denoised original sample data to near-field millimeter-wave cylindrical scanning reconstruction algorithm to achieve the three-dimensional space scattering intensity distribution of the targets.

## 3. EXPERIMENTS

The actual near-field millimeter-wave cylindrical scanning imaging system is shown in Figure 2(a). The antenna array of the imaging system is driven by motor to complete  $360^\circ$  high-speed scanning. The angle step is  $\Delta\theta = 0.3^\circ$ , and the sample point along  $\theta$  direction is 1200. The transceiver channel number

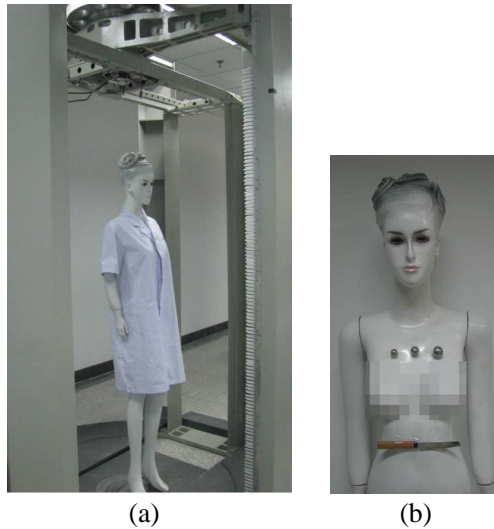


**Figure 2.** Experiment system. (a) Imaging system. (b) Test targets.

of antenna array is 256, and the sample point along  $z$  direction is 256. The system frequency band is from 20 GHz to 30 GHz, and the sample point along  $\omega$  direction is 200. The targets under test in the experiments are three metallic balls and a knife, which are placed on the body of a plastic mannequin, as shown in Figure 2(b). The diameters of the three metallic balls from left to right are 1 cm, 1.5 cm and 2 cm, respectively. The test targets are placed in the center of the imaging system.

The scattering information of the measured targets in the imaging system is corresponding to each sample position and step frequency. The sampled three-dimensional matrix of scattering information can be decomposed into frequency, height and angle directions. In order to show the noise floor of the imaging system, we choose a small part of the three-dimensional matrix, which includes 50 sample points along  $\theta$  directions and 200 sample points along  $\omega$  direction. Range profiles are used to examine the denoising effect of the denoising algorithm with the pulse noise model, white Gaussian noise model and the plus noise model, as shown in Figure 3. After power normalization, the noise floor of original sample data focuses on  $-40$  dB. The white Gaussian noise model and the plus noise model are more effective in denoising the system noise. The noise floor of the imaging system is reduced more than 20 dB compared with the original sample data. The Pulse noise model has only a little denoising effect, the noise floor is reduced only about 3 dB compared with the original sample data.

The discussion above is mainly focused on the one dimensional range profiles. In order to check the denoising effect in three-dimensional imaging, the original sample data and denoised data with the plus model are applied in near-field millimeter-wave cylindrical scanning three-dimensional reconstruction algorithm. The three-dimensional space scatter intensities of the three metallic balls are shown in Figure 4.

The denoising effect of the three-dimensional space scatter intensities are corresponding with the denoising effect of range profiles. As expected, when the plus noise model is applied, the noise floor of space scatter intensity is reduced more than 10 dB. After three-dimensional reconstruction of the

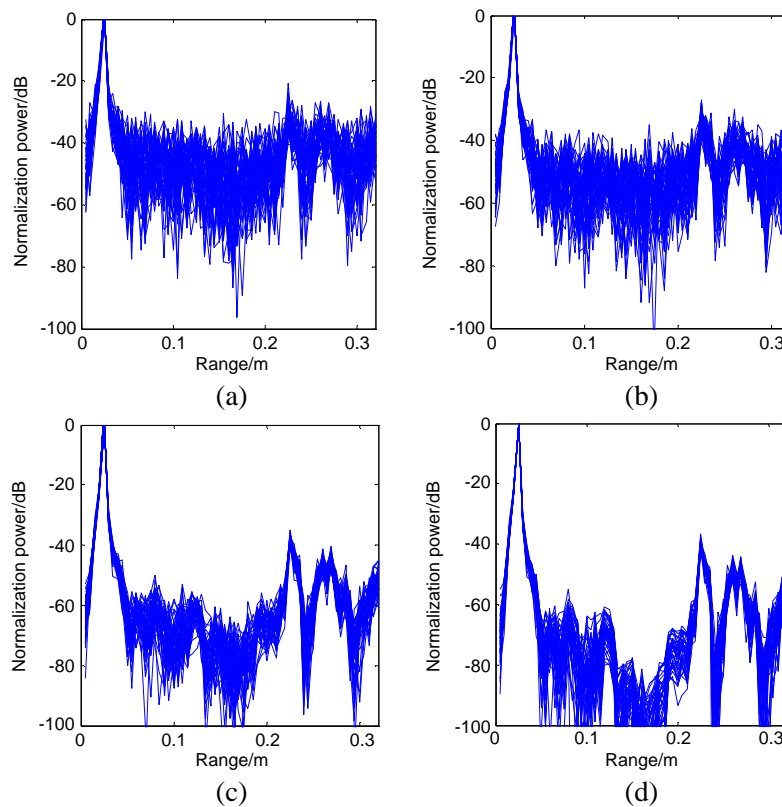


**Figure 3.** The denoising effect of range profiles. (a) Original sample data. (b) Pulse noise model. (c) White Gaussian noise model. (d) The plus model.

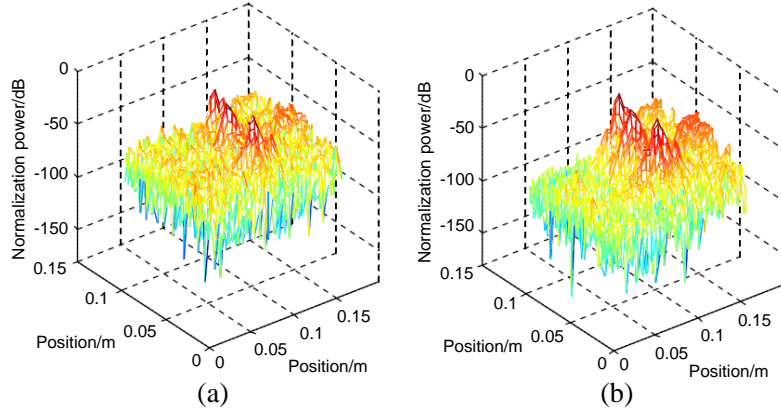


**Figure 4.** The scatter intensity of three mental balls. (a) Original sample data. (b) The plus model.

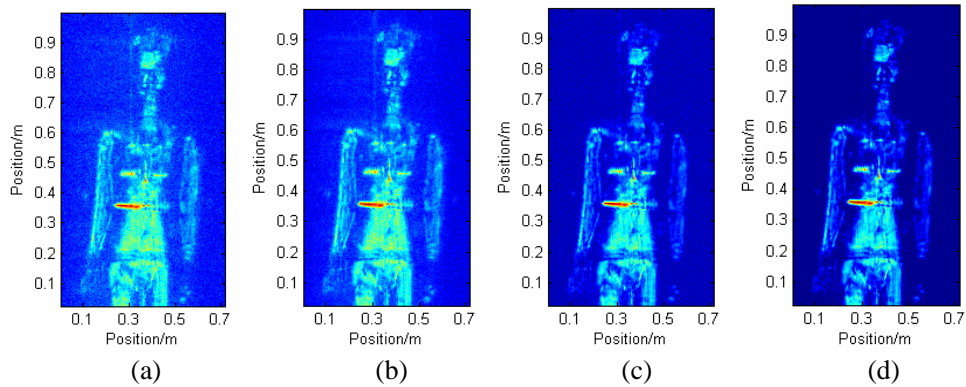


**Figure 5.** Imaging results of different noise model. (a) Original sample data. (b) Pulse noise model. (c) White Gaussian noise model. (d) The plus model.

test targets, two-dimensional images are achieved by projecting the three-dimensional scatter intensity along forward, which are shown in Figure 5. When the original sample data or the pulse noise model are applied, the clarity of two-dimensional image is poor, the boundary between the mannequin and background is not clear and the contours of the test targets are blurring. When the white Gaussian noise model or the plus model is applied, improvements are observable.

#### 4. CONCLUSIONS

The major contribution of this article is the development of the ICA denoising algorithm in near-field millimeter-wave cylindrical scanning imaging system. The algorithm applies three different noise models to expand the original sample data, and the sources can be effectively separated from the noise by the ICA denoising algorithm. Experiment results demonstrate that when applying the appropriate noise model in the ICA model, the noise floor of the system can be obviously reduced. On account of the fact that the noise components of the imaging system are very complex, we have to research more accurate noise models in the future.

#### REFERENCES

1. Soumekh, M., "Reconnaissance with slant plane circular SAR imaging," *IEEE Trans. on Image Processing*, Vol. 5, No. 8, 1252–1265, 1996.

2. LaHaie, I. J. and E. I. LeBaron, "Processing techniques for removal of target support contamination," *AP-S. Digest Antennas and Propagation Society International Symposium*, Vol. 1, 488–491, 1993.
3. Burns, J. W. and N. S. Subotic, "Reduction of clutter contamination in radar cross section measurements using independent components analysis," *IEEE Antennas and Propagation Society International Symposium*, Vol. 1, 731–734, 2004.
4. LaHaie, I. J., "An overview of advanced processing techniques for RCS measurements," *IEEE Antennas and Propagation Society International Symposium*, Vol. 4, 608–611, 2001.
5. Kristensson, G. and M. Gustafsson, "Measuring the extinction cross section," *3rd European Conference on Antennas and Propagation, EuCAP 2009*, 3633–3636, 2009.
6. Hilliard, D. and L. To, "Advanced radar cross section clutter removal algorithms," *2010 Proceedings of the Fourth European Conference on Antennas and Propagation (EuCAP)*, 1–5, 2010.
7. Piere, C., "Independent component analysis, a new concept," *Signal Processing — Special Issue on Higher Order Statistics*, Vol. 36, No. 3, 287–314, 1994.
8. Miller, E. G. and W. John, "ICA using spacings estimates of Entropy," *Journal of Machine Learning Research*, Vol. 4, Nos. 7–8, 1271–1295, 2003.
9. Cardoso, J. F. and A. Souloumiac, "Blind beamforming for non-Gaussian signals," *IEE Proceedings — Radar and Signal Processing*, Vol. 140, No. 6, 362–370, 1993.
10. Murillo-Fuentes, J. J. and F. J. Gonzalez-Serrano, "Independent component analysis with sinusoidal fourth-order contrasts," *Acoustics, Speech, and Signal Processing*, Vol. 5, 2785–2788, 2001.
11. Hyvarinen, A., "Survey on independent component analysis," *Neural Computing Surveys*, Vol. 2, 94–128, 1999.
12. Hyvarinen, A. and E. Oja, "Independent component analysis: Algorithms and application," *Neural Networks*, Vol. 13, 411–430, 2000.
13. Hyvarinen, A., "Gaussian moments for noisy independent component analysis," *IEEE Signal Processing Letters*, Vol. 6, No. 6, 145–147, 1999.
14. Giannakis, G. and S. Shamsunder, "Modelling of non-Gaussian array data using cumulants: DOA estimation of more sources with less sensors," *Signal Processing*, Vol. 30, No. 3, 279–297, 1993.
15. Jiao, W. D. and S. X. Yang, "Study of noise removal techniques based on independent component analysis," *Journal of Zhejiang University*, Vol. 38, No. 7, 872–876, 2004.